Design rules for interfacial thermal conductance: Building better bridges

Carlos A. Polanco,[1,*] Rouzbeh Rastgarkafshgarkolaei,[2] Jingjie Zhang,[1] Nam Q. Le,[2] Pamela M. Norris,[2] and Avik W. Ghosh[1,3,†]

[1]*Department of Electrical and Computer Engineering, University of Virginia, Charlottesville, Virginia 22904, USA*

[2]*Department of Mechanical and Aerospace Engineering, University of Virginia, Charlottesville, Virginia 22904, USA*

[3]*Department of Physics, University of Virginia, Charlottesville, Virginia 22904, USA*

(Received 20 August 2016; revised manuscript received 26 January 2017; published 3 May 2017)

We study the thermal conductance across solid-solid interfaces as the composition of an intermediate matching layer is varied. In the absence of phonon-phonon interactions, an added layer can make the interfacial conductance increase or decrease depending on the interplay between (1) an increase in phonon transmission due to better bridging between the contacts and (2) a decrease in the number of available conduction channels that must conserve their momenta transverse to the interface. When phonon-phonon interactions are included, the added layer is seen to aid conductance when the decrease in resistances at the contact-layer boundaries compensate for the additional layer resistance. For the particular systems explored in this work, the maximum conductance happens when the layer mass is close to the geometric mean of the contact masses. The surprising result, usually associated with coherent antireflection coatings, follows from a monotonic increase in the boundary resistance with the interface mass ratio. This geometric mean condition readily extends to a compositionally graded interfacial layer with an exponentially varying mass that generates the thermal equivalent of a broadband impedance matching network.

DOI: 10.1103/PhysRevB.95.195303

I. INTRODUCTION

Nanostructured materials offer unprecedented opportunities for thermal management and energy conversion by enabling a wider range as well as better control of the thermal conductivity [1–4]. Interfaces are central to their performance since they are scattering centers for heat carriers whose spatial distribution can be set during fabrication and whose dispersion strength can be controlled by tailoring their physical properties [5–8]. Nevertheless, the full potential of this revolution is still to be seen because there is a gap between our fundamental understanding of heat flow across single and multiple interfaces and the outcome of experimental measurements [6]. For instance, while many simulations predict an enhancement of thermal conductance when a thin layer is inserted at a well bonded interface [9–15], only one experiment backs up that prediction so far [16]. Other experiments reporting conductance enhancement attribute the increase to a strengthening of the bonds at the boundaries [17–19]. Thermal interface engineering can be critical to many technologies like integrated circuits [3], phase change memory [20], or high power electronics [21]. A systematic and microscopic understanding of the bridging properties of an interfacial layer would go a long way towards that goal.

Adding an intermediate layer to a well-bonded interface can enhance the conductance in two different ways. In the harmonic limit, the layer could act as an impedance matching waveguide [Fig. 1(a)] that reduces phonon reflection by destructive interference, similar to an antireflection coating [22]. Such a complete quenching of reflection occurs at a single frequency where the layer thickness can function as a quarter wave plate. In the anharmonic regime on the other hand, the layer can act as a bridge that facilitates frequency up and down conversion and increases the chances of phonons crossing the interface [12] [Fig. 1(b)].

The contribution of each individual effect to the total enhancement has not been systematically explored on the same material system. Neither is there a clear criterion to choose the properties of the layer to maximize the conductance. In a 1D harmonic crystal for instance, we have established that a conductance maximum occurs when the impedance of the layer is the geometric mean of the contact impedances [22], even in the presence of incoherent interface scattering. This thumb rule persists for all lengths except the extreme limit of a single atom, where the mean generates a resonance that lies beyond the cutoff frequency and the system is forced to choose an arithmetic mean instead [23,24]. However, this result has not been extended to multiple dimensions and crystal structures. A similar gap exists when phonon-phonon interactions are included, where it was proposed that the maximum conductance happens when the layer's density of states (DOS) maximizes its overlap with the contact DOSs. This argument leads to two different criteria to obtain the maximum: (1) choose the atomic mass of the layer close to the arithmetic mean of the contact masses [12] and (2) choose the Debye temperature of the layer as the geometric mean of the contact Debye temperatures [11]. This unresolved discrepancy once again reveals our lack of understanding of the role played by the inserted layer for a real multidimensional physical system with complex modes, symmetries, and scattering events.

Design rules to choose the properties of the intermediate layer that maximize interfacial conductance are still missing. For instance, although the conductance depends on the thickness [22,25], crystallinity [26], and bonding strength [27] of the inserted layer, it is not clear how to choose those properties to maximize the conductance. It is also unclear how to design the properties of graded layers. A recent study showed a large enhancement of interfacial conductance when the mass of the layer is varied linearly [28]. This opens a

*cap3fe@virginia.edu

†ag7rq@virginia.edu

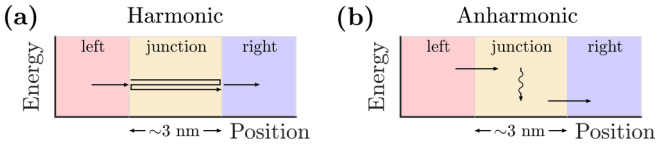

FIG. 1. Interface with an added intermediate layer or junction (bridged interface). (a) In the harmonic limit, the layer behaves like an impedance matcher that increases transmission by constructive interference while reducing the number of conducting modes due to energy-momentum conserving constraints. (b) In the anharmonic limit, the layer behaves as a bridge for phonon down and up conversion that increases the chances of phonons crossing the interface.

new gamut of design possibilities, and the potential for further conductance enhancement needs to be explored.

In this paper we compare the enhancement of conductance in the harmonic and anharmonic limits and demonstrate the dominant role of anharmonicity (Sec. II). We show that adding an intermediate layer can go either way by increasing or decreasing the conductance when phonon transport is restricted to the harmonic regime (Sec. III). In this limit, the conservation of energy and momentum constrain the number of available transport channels, so the increase in average transmission per channel must compete with the loss in the number of transport channels. When anharmonicity is added (Sec. IV), phonon-phonon interaction relaxes the conservation constraints and decouples the boundaries. Maximizing the conductance becomes equivalent to minimizing the sum of individual boundary resistances. For our particular system, where only mass changes are considered, we show that the maximum happens when the layer mass is close to the geometric mean of the contact masses. As explained earlier, this result would be expected for 1-D coherent phonon transport at a single frequency. The surprise however is that the geometric mean ends up winning even for a 3-D crystal with broad-band phonon transport across modes and polarizations, including anharmonic and diffusive interactions. We can hypothesize that a bridging layer can in fact be a matching layer if we compositionally grade it so each slice has an acoustic impedance that is the geometric mean of its immediate nearest neighbors. The tendency of the geometric mean to favor the lower impedance of the pair mathematically translates to an exponentially varying spatially dependent impedance, with an exponent set by the logarithm ratio of the two impedances at either end of the layer.

II. HARMONIC VS ANHARMONIC ENHANCEMENT OF G

Interface thermal conductance or thermal boundary conductance is defined as the ratio between the heat flux crossing an interface over the temperature drop across it, $G = q/\Delta \boldsymbol{T}$. Within the Landauer formalism, the conductance between two contacts at thermal equilibrium can be expressed as [29]

$$G = \frac{1}{A}\int_0^\infty \frac{d\omega}{2\pi}\hbar\omega\frac{\partial N}{\partial \boldsymbol{T}}MT \xrightarrow{\hbar\omega<<k_B\boldsymbol{T}} \frac{k_B}{2\pi A}\int_0^\infty d\omega MT, \tag{1}$$

where A is the cross sectional area, $\hbar\omega$ is the phonon energy, N is the Bose-Einstein distribution, k_B is the Boltzmann constant, M is the number of available propagating channels, which we call modes, and T is the average transmission per mode. In a bulk material, each mode is a 1D subband generated by a particular polarization and a transverse wave vector, which gives rise to a quantum of conductance [30]. The factor MT represents the sum of all the possible transmissions between the modes on the left and right contacts. This factor can be calculated using nonequilibrium Green's functions (NEGF) as $MT = \mathrm{Trace}\{\Gamma_l G_r \Gamma_r G_r^\dagger\}$, with G_r the retarded Green's function describing the propagation of phonon waves in the channel and $\Gamma_{l,r}$ the broadening matrix for the left (l) and right (r) contacts [30–32]. To compare the conductance from Landauer formalism with that from nonequilibrium molecular dynamics (NEMD), we need to take the classical limit of the Bose-Einstein distribution [Eq. (1) with $\hbar\omega \ll k_B\boldsymbol{T}$] and we need to subtract the contact resistance [Appendix B and Fig. 3(b)]. This value should be the limit of the NEMD conductance as temperature tends to zero.

Figure 2 plots the harmonic and anharmonic thermal conductances G^B across interfaces with an added intermediate bridging layer or junction, belonging to a face centered cubic (FCC) crystal structure in one case and diamond cubic (DC) in the other. The boundaries between adjacent materials are assumed to be perfectly abrupt and the thickness of the junction is taken to be six conventional unit cells. For each system, we vary the atomic mass of the junction m_j in between the contact atomic masses m_l and m_r. We assume that the crystal structure, lattice constant a, and interatomic force constants are invariant along the system, so we can isolate the effect of a change in atomic mass. Some consequences of relaxing

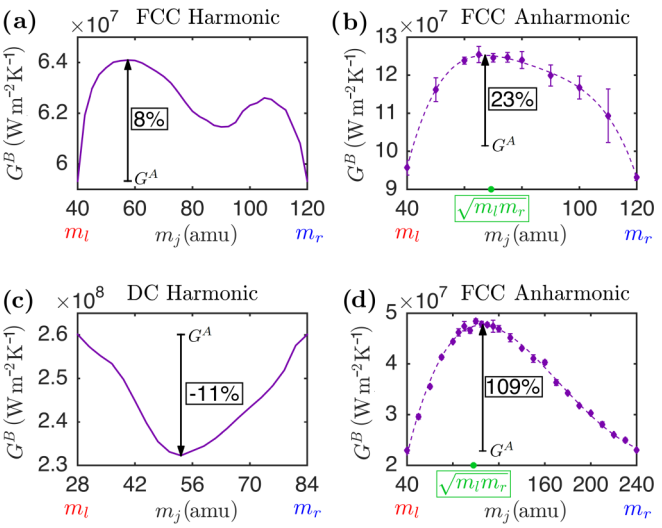

FIG. 2. Conductance of bridged interfaces as the atomic mass of the intermediate layer or junction is varied between the contact masses. The conductance of the abrupt interface is indicated by the tail of the arrow. In the harmonic limit, a FCC crystal shows a relative enhancement of conductance from abrupt to bridged interface (a), while a DC crystal shows the opposite (c). In the anharmonic regime (b), the conductance enhancement of a FCC crystal is three times larger than that of the harmonic limit (a). Moreover, the maximum enhancement happens when the junction mass is close to the geometric mean of the contact masses (c) $m_r = 120$ amu and (d) $m_r = 240$ amu. The dashed lines are fourth order polynomial functions that fit the NEMD data.

these assumptions are discussed at the end of each of the following sections. The conductance in the harmonic regime is calculated from Landauer formalism in the classical limit using NEGF to obtain MT, while the conductance in the anharmonic regime is calculated from NEMD. Note that we report the conductance measured from the left to the right material including the contribution from the junction. Thus, the abrupt interface conductance from NEMD is larger than that of the bridged interface when the junction mass is equal to one of the contact masses. Those conductance values from Landauer formalism are equal because the calculations are harmonic. The details of the simulations are spelled out in Appendix A.

Figures 2(a) and 2(b) suggest that anharmonicity plays a key role in the relative enhancement of conductance from an abrupt (superscript A) to a bridged (superscript B) interface. The anharmonic simulations show a relative increase in conductance $[\Delta G = (G^B - G^A)/G^A = 23\%$ at $\boldsymbol{T} = 30$ K] three times larger than that of the harmonic simulations ($\Delta G = 8\%$ at $\boldsymbol{T} = 0$ K). This difference cannot be explained in terms of the usual linear increase of conductance with temperature shown by NEMD simulations of abrupt interfaces [Fig. 3(a)] [9,33,34]. In fact, the maximum conductance of bridged interfaces increases nonlinearly with temperature [Fig. 3(a)], with a rapid growth at low temperatures. This suggests the existence of a mechanism that limits the conductance enhancement just in the harmonic regime. In Sec. III, we explain that the limiting mechanism arises from the conservation of phonon energy and transverse momentum, which constrains the number of available transport channels across the interface. We also show that for certain crystal structures, this mechanism can even destroy the conductance enhancement of bridged interfaces over abrupt interfaces [Fig. 2(c)].

In the limit of zero temperature, the conductances calculated from Landauer and NEMD methods are in excellent agreement [Fig. 3(a)]. The Landauer conductance is defined using the temperature drop between contacts at thermal equilibrium $G_L = q/\Delta \boldsymbol{T}_c$. Therefore, it *includes* additional resistances at the contacts that arise from the implicit scattering assumed to bring the distribution of phonons back to equilibrium

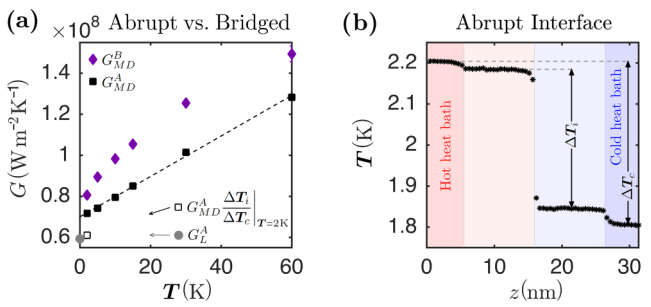

FIG. 3. (a) Conductance of the abrupt interface G^A_{MD} and maximum conductance of the bridged interface G^B_{MD} vs temperature for a FCC crystal calculated from NEMD. The rapid increase of G^B_{MD} at low $\boldsymbol{T}$ highlights the important role of anharmonicity enhancing G^B_{MD} relative to G^A_{MD}. (b) Temperature profile of the abrupt interface from NEMD. This profile allows us to include the contact resistances into the NEMD conductance [Eq. (2)], which shows excellent agreement with our Landauer calculations G^A_L.

(Appendix B). On the other hand, the NEMD conductance is defined using the temperature drop right at the interface $G_{MD} = q/\Delta \boldsymbol{T}_i$ [Fig. 3(b)], so it *excludes* the resistances at the contacts. Those resistances cause the temperature drops at the boundaries of the heat baths [Fig. 3(b)], where thermal equilibrium is enforced. When we include the contact resistances into the NEMD conductance [right hand side of Eq. (2)], we get the Landauer conductance

$$G_L = \lim_{\boldsymbol{T}\to 0} G_{MD} \frac{\Delta \boldsymbol{T}_i}{\Delta \boldsymbol{T}_c}. \tag{2}$$

Figure 3(a) shows an example of the excellent agreement of the two conductances once we account for the effects of the contact resistances.

In the anharmonic regime, our simulations show that the conductance enhancement is maximum when the junction mass is close to the geometric mean of the contact masses $m_j \approx \sqrt{m_l m_r}$ [Figs. 2(b) and 2(d)]. This result is a consequence of the boundary resistance being an increasing function of the mass ratio of the materials at either side of the boundary (Sec. IV). Therefore, the sum of the boundary resistances is minimum when the ratio of the masses is equal ($m_j/m_l = m_r/m_j \to m_j \approx \sqrt{m_l m_r}$). Notably, this is a much more general result than an antireflection coating, which requires in addition a quarter wave plate to not just minimize but completely eliminate the sum of the boundary resistances through destructive interference, that only works at a single frequency for a homogeneous layer material.

III. HARMONIC LIMIT: INCREASING TRANSMISSION VS DECREASING CONSERVING MODES

When phonons transit without interacting with each other, adding an intermediate layer does not necessarily increase the interfacial conductance [Fig. 2(c)]. This result challenges our intuition of maximizing wave transmission at an interface by impedance matching. Recently, we demonstrated in 1D systems that adding an intermediate material with impedance equal to the geometric mean of the contact impedances maximizes the transmission over the broadband spectrum of phonons and therefore maximizes the thermal conductance at the interface [22]. We even showed that an impedance of the intermediate layer between the impedances of the contacts enhances the interfacial thermal conductance [22]. Based on those results, we would expect that adding an intermediate material to either the FCC or DC abrupt interface would enhance the interfacial thermal conductance. However, Fig. 2 shows that this hypothesis is not correct. While we see an enhancement in the FCC interface we see a decrease in the DC crystal.

To understand this result, we start by rewriting Eq. (1) to highlight the role of phonon transmission vs number of transport channels on the interfacial conductance. G is related to the factor MT, which represents the sum over all the possible phonon transmissions between modes of the left contact, junction, and right contact. Due to the perfectly abrupt nature of the boundaries, the system is periodic in the transverse direction, so that successful transmissions must conserve the transverse wave vector ($k_\perp$). We rewrite MT to highlight the

factors contributing to transport as

$$MT = \sum_{T_{k_\perp}\neq 0} T_{k_\perp} = M_c \left[\frac{1}{M_c} \sum_{T_{k_\perp}\neq 0} T_{k_\perp} \right] = M_c T_c, \quad (3)$$

where $k_\perp$ varies over the transverse Brillouin zone, the conserving modes M_c counts the number of nonzero transmissions or transport channels across the interface, and T_c is the average transmission over the conserving modes [15]. Using these definitions, we can rewrite the conductance as

$$G = G_{M_c} \langle T_c \rangle_\omega, \quad (4)$$

with the contribution to the conductance by the conserving modes G_{M_c} given by

$$G_{M_c} = \frac{1}{A} \int_0^\infty \frac{d\omega}{2\pi} \hbar\omega \frac{\partial N}{\partial \boldsymbol{T}} M_c \xrightarrow{\hbar\omega << k_B \boldsymbol{T}} \frac{k_B}{2\pi A} \int_0^\infty d\omega M_c \quad (5)$$

and $\langle T_c \rangle_\omega = G/G_{M_c}$.

To calculate M_c numerically, we find the propagating modes of the bulk left contact (M_l), junction (M_j), and right contact (M_r) by calculating MT from NEGF for each homogeneous material, where $T_{k_\perp} = 1$ for each mode and 0 otherwise. Then, the conserving modes are computed from

$$M_c(\omega) = \sum_{k_\perp} \min[M_l(\omega, k_\perp), M_j(\omega, k_\perp), M_r(\omega, k_\perp)]. \quad (6)$$

Note that M_c is a concept similar in spirit to the diffuse mismatch model [35], since it depends only on the bulk properties of each individual material. Also note that we are assuming that tunneling across the junction is negligible, which is reasonable for junctions larger than four atomic layers. This assumption allows us to consider only transmissions involving propagating channels of the junction.

The relative enhancement in the conductance of a bridged (superscript B) interface compared to that of an abrupt (superscript A) interface depends on the interplay between increasing the transmission and decreasing the conserving modes. Figure 4 compares the relative change in conductance,

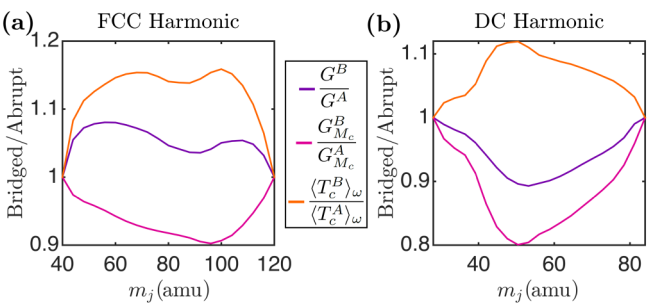

FIG. 4. In the harmonic limit, the conductance of a bridged interface results from an interplay between increasing the transmission $\langle T_c \rangle_\omega$ due to decreasing the "mismatch" at each boundary and decreasing the number of conserving modes due to a new restriction on the conservation of momentum coming from the intermediate material.

conserving modes and transmission using

$$\frac{G^B}{G^A} = \left[\frac{G^B_{M_c}}{G^A_{M_c}} \right] \left[\frac{\langle T_c^B \rangle_\omega}{\langle T_c^A \rangle_\omega} \right], \quad (7)$$

with M_c for the abrupt interface defined analogous to Eq. (6), but the minimum is taken only over the contact modes. For the FCC crystal [(Fig. 4(a)], the increase in transmission is enough to counter balance the decrease in modes. However, for the DC crystal [Fig. 4(b)], the decrease in modes dominates and pushes the conductance of the bridged interface below that of the abrupt interface. Figure 4 shows that the transmission ratio $\langle T_c^B \rangle_\omega / \langle T_c^A \rangle_\omega$ is larger than one for both systems, so it is trying to enhance G_B/G_A, while the conductance ratio due to the conserving modes, $G^B_{M_c}/G^A_{M_c}$, is less than one for both systems, so it is trying to abate G_B/G_A. Thus, adding the intermediate layer enhances the transmission of individual phonons, as expected from our intuition of impedance matching, but it also decreases the number of available transport channels to cross the interface. That is, the interplay between transmission and number of modes is a competition between increasing the value of individual transmitting channels vs decreasing the number of them.

Note that the minimum conductance ratio G_B/G_A of the DC system happens when the transmission ratio is a maximum ($\approx$1.12). This value is similar to the maximum transmission ratio of the FCC system ($\approx$1.15). However, the minimum ratio of conductance due to the conserving modes $G^B_{M_c}/G^A_{M_c}$ is around 0.8 for the DC system and 0.9 for the FCC system. Therefore, $G^B_{M_c}/G^A_{M_c}$ is the key factor to distinguish between the maximum and minimum conductance of the FCC and DC systems, respectively.

We can design an intermediate bridging layer at an abrupt interface to improve the impedance matching and increase the mode averaged transmission; however, it is important to note that an added layer always decreases the number of modes available for transport. This is a consequence of the need to conserve phonon energy and transverse momentum in three materials instead of two, which implies taking the minimum over three quantities instead of two [Eq. (6)]. The extra constraint is more noticeable around frequencies where $M_j < \min(M_l, M_r)$. For instance, Fig. 5(b) shows a reduction of the conserving modes of the bridged interface relative to those of the abrupt interface around 4 and 6×10^{13} rad/s. Note that at low frequencies, the acoustic branches of the lightest material dominate the conserving modes and $M_c^A \approx M_c^B$. Thus, at low temperatures we expect $G^B > G^A$ for both crystal structures, FCC and DC, since $\langle T_c^B \rangle_\omega > \langle T_c^A \rangle_\omega$.

As long as the system remains periodic in the transverse direction, i.e., invariant lattice constant and perfectly abrupt boundaries between adjacent materials, the concepts developed in this paper apply. However, when the transverse symmetry assumption is relaxed, for example when the lattice constants are not the same or when there are random defects or interatomic mixing at the interface, phonons can change their momentum when they cross the interface. Therefore, the conserving modes do not represent anymore the available transport channels or modes across the interface. The number of transport channels is intimately related to the properties of the individual boundaries between adjacent materials, like the

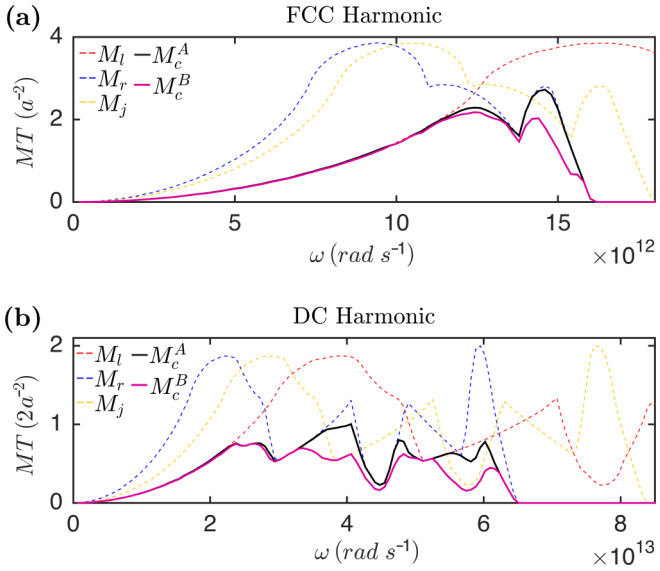

FIG. 5. Available modes for the contacts and junction, and conserving modes of the bridged and abrupt interface. Adding the junction puts an extra constraint on the conserving modes that hurts M_c and decreases the number of available modes. We plot the cases in which G_{M_c} is minimum: $m_j = 96$ amu for the FCC crystal and $m_j = 50.4$ amu for the DC crystal.

degree of interatomic mixing. In that case, conservation of energy allows us to define an upper bound for MT [15],

$$MT^B(\omega) \leqslant \min(M_l(\omega), M_j(\omega), M_r(\omega)) = M^B_{\min}, \quad (8)$$

which can be used as a measure of the number of transport channels. Similar to the conserving modes, the minimum of the modes always decreases when a junction is added to an abrupt interface, because we are taking the minimum of three quantities instead of two (Fig. 5).

The conserving modes M_c and minimum of the modes $M_{\min}$ can be convenient starting points to look for junction materials that could enhance interfacial conductance. For instance, the combinations of materials that maximize M_c or $M_{\min}$ should be more amenable to increases in interfacial conductance.

IV. ANHARMONIC LIMIT: DECREASING BOUNDARY RESISTANCE VS INCREASING JUNCTION RESISTANCE

When phonons interact with each other during transport across the junction, for instance through anharmonic terms in the channel potential, they change their energy and momentum. This process relaxes the conservation constraints in the harmonic limit and decouples the system resistance as the sum of boundary resistances plus a junction resistance

$$R = R_{lj} + R_j + R_{jr}. \quad (9)$$

The added intermediate layer will enhance the interfacial conductance when the system resistance [Eq. (9)] is less than the resistance of the abrupt interface between the left and right contacts, R_{lr}, that is when $R = R_{lj} + R_j + R_{jr} < R_{lr}$. The validity of this inequality depends on how fast the boundary resistances decrease as the mismatch of the materials decreases.

Figures 2(b) and 2(d) suggest that the maximum conductance, or minimum resistance, happens when the junction mass is close to the geometric mean of the contact masses. A similar result in terms of impedances was found for the analog one-dimensional system, where phonon transport was elastic but incoherent [22]. The key element behind the result was that each boundary resistance is an increasing function of the impedance ratio of the materials at either side of the boundary. Thus, minimizing the sum of resistances requires equating the impedance ratios ($Z_j/Z_l = Z_r/Z_j \rightarrow Z_j = \sqrt{Z_l Z_r}$). Inspired by this result, it is tempting to suggest that G is a function of the mass ratio alone. Unfortunately this is not true because heavier materials yield lower conductances due to their smaller cutoff frequencies, which can be seen by rewriting Eq. (1) as

$$G = \frac{k_B}{2\pi A}\omega_{\min}\langle MT\rangle_\omega, \quad (10)$$

with $\omega_{\min}$ the minimum cutoff frequency of the contacts $\omega_{\min} = \min(\omega_{cl}, \omega_{cr})$ and

$$\langle MT\rangle_\omega = \frac{1}{\omega_{\min}}\int_0^\infty d\omega MT. \quad (11)$$

Although the boundary conductance is not a function of the mass ratio alone, the conductance over the frequency cutoff $G/\omega_{\min}$ is. Figure 6(a) shows that $\langle MT\rangle_\omega$ is only a function of the mass ratio for both the anharmonic and harmonic limits. The anharmonic data results from combining Eq. (10) with the boundary conductance extracted from our NEMD simulations. The data from the boundary between the left contact and the junction (red triangles) is a little larger than that from the boundary between the junction and the right boundary (blue triangles), because the temperature is greater at the left boundary. The harmonic data comes from the Landauer conductance after we have subtracted the contact resistances (Appendix B). If that is not the case, we obtain the dashed line in Fig. 6(a), which is bounded for unity mass ratio due to the resistances at the contacts.

Replacing the boundary resistances ($R = 1/G$) from Eq. (10) into Eq. (9) and using $\langle MT\rangle_\omega$ from Landauer [solid line in Fig. 6(a)], we numerically find the junction mass that maximizes interfacial conductance as a function of the ratio of the contact masses [solid line Fig. 6(b)]. The noise in the plot is caused by the interpolation error in $\langle MT\rangle_\omega$. The fair agreement

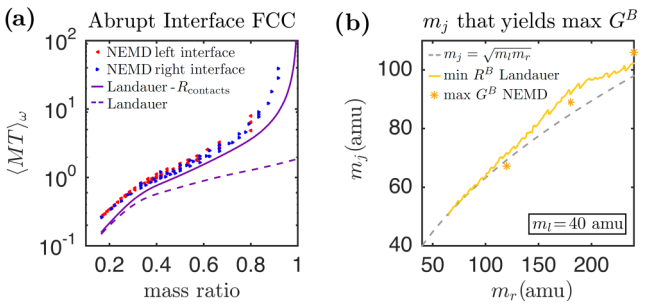

FIG. 6. (a) $\langle MT\rangle_\omega$, plotted per conventional unit cell, is a function of the mass ratio for abrupt interfaces. (b) Junction mass m_j that leads to minimum resistance vs right contact mass m_r while keeping the left contact mass fixed. The mass follows closely the geometric mean of the contact masses.

of this curve with the results from NEMD simulations [Figs. 2(b) and 2(d)] suggests that the knowledge of the harmonic boundary conductance is enough to approximate the junction mass that maximizes the conductance. Nevertheless, one of the reasons behind the discrepancy is the flattening of the curve around the peak [Figs. 2(b) and 2(d), Appendix A, and Fig. 8), which combined with the uncertainty of the NEMD results produces a corresponding spread in the maximum. In fact, the large spread of the conductance maximum and its relative insensitivity around that point with changes of junction mass is quite convenient for engineering, as it widens our choice of bridging masses that yield an overall large conductance.

The solid curve in Fig. 6(b) follows closely the geometric mean of the contact masses (dashed line) due to the dominant dependance of G on the mass ratio. The deviations from this mean arise from the dependence of G on the overall phonon cutoff frequency $\omega_{\min}$, which adds a more complicated mass dependence. We can better understand the trend of maximum conductance by minimizing Eq. (9)

$$\frac{\partial R}{\partial m_j} = \frac{2\pi A_{cu}}{k_B \omega_{cr}} \left[\frac{F_{lj}}{2\sqrt{m_j m_r}} - \sqrt{\frac{m_j}{m_r}} \underbrace{\frac{m_l}{m_j^2} F'_{lj}}_{\text{term } \alpha} + \underbrace{\frac{1}{m_r} F'_{jr}}_{\text{term } \beta} \right] = 0. \tag{12}$$

To obtain Eq. (12) we use $m_l < m_j < m_r$, Eq. (10), $F_{lj} = \langle MT(m_l/m_j)\rangle^{-1}$, $F_{jr} = \langle MT(m_j/m_r)\rangle^{-1}$, F' the derivative of F with respect to m_j, and we neglect $\partial R_j/\partial m_j$. We also express the cutoff frequencies of the junction ω_{cj} and right contact ω_{cr} in terms of the cutoff frequency of the left contact ($\omega_{cj} = \omega_{cl}\sqrt{m_l/m_j}$, $\omega_{cr} = \omega_{cl}\sqrt{m_l/m_r}$). This is possible because the materials are identical except for the atomic mass, so the dispersion is a copy of the same function expanded or contracted along the frequency axis. A_{cu} is the area of the conventional unit cell that converts the value of $\langle MT\rangle_\omega$ per conventional unit cell in Fig. 6(a) to per meter squared. When the ratio between the contact masses is close to one, choosing the junction mass close to the geometric mean of the contact masses maximizes the conductance [Fig. 6(b)]. In that case, $\sqrt{m_j/m_r} \approx 1$, $F_{lj} \approx 0$ and Eq. (12) reduces to the terms α and β. This expression is minimum when $m_j \approx \sqrt{m_l m_r}$. As the ratio of the contact masses increases, the junction mass that maximizes the conductance remains close to the geometric mean. This happens because the deviation of the second term relative to the term α, caused by $\sqrt{m_j/m_r} < 1$, is balanced to some extent by the increase of F_{lj} on the first term (note that F' is negative).

To minimize the resistance, (1) we assume the boundary resistances are in series, (2) we show the boundary conductance is an increasing function of the mass ratio, and (3) we conclude that the minimum resistance happens when the mass ratios are equal. This strategy can be used beyond systems with perfect boundaries where only the mass is allowed to change. We expect the same minimization outcome, $m_j \approx \sqrt{m_l m_r}$, when interatomic mixing is added at the boundaries. Mixing can either suppress [5] or enhance [12,13,15] each boundary conductance. Either way, we still expect a similar increasing trend of $\langle MT\rangle_\omega$ with mass ratio dictated by the frequency minimum of the modes $M_{\min}$ instead of the conserving modes M_c [15]. By analogy, if we only allow changes of the interatomic force constants by varying the ϵ parameter of the Lennard-Jones potential, we expect minimum resistance when $\epsilon_j \approx \sqrt{\epsilon_l \epsilon_r}$. Although the force constants and masses have opposite effects on the cutoff frequency, we still expect $\langle MT\rangle_\omega$ to be an increasing function of the ϵ ratio. When we allow changes of both the masses and force constants, a similar analysis suggests that the minimum resistance happens when $m_j/\epsilon_j \approx \sqrt{m_l m_r/\epsilon_l \epsilon_r}$. Further studies are necessary to confirm our hypotheses and to extend it to matrix versions of m and ϵ for anisotropic systems.

We expect further enhancement of the conductance between the contacts by stacking several intermediate thin layers whose atomic masses change in an exponential fashion. This result follows from choosing the mass of each layer as the geometric mean of the masses of the adjacent layers. Each geometric mean choice minimizes the sum of the boundary resistances adjacent to a particular layer. A similar conjecture has been demonstrated for 1D incoherent systems [15].

The assumption that anharmonicity allows us to split the system resistance as the sum of resistances [Eq. (9)] is supported by our simulations. Figures 6 and 8 compare quantities obtained from NEMD simulations of the whole interface, which include the correlation between the two contact-layer boundaries, with quantities obtained by manipulating results from NEGF simulations on a single independent boundary. The similarity between the $\langle MT\rangle_\omega$ trends in Fig. 6(a) suggests that the $\langle MT\rangle_\omega$ extracted from NEMD at each layer-contact boundary is mostly independent of the other boundary. Thus, the boundary resistances [Eq. (10)] are independent of each other. Those independent resistances can be added to obtain the total resistance according to the temperature profile used to define them, where the total temperature drop across the interface is the sum of the drop at each boundary plus the drop at the intermediate layer. The similarity of the trends of G vs m_j in Fig. 8 suggests that the correlation of the two interfaces is playing a minimal role and that the trend of G vs m_j is well described by the sum of independent boundary resistances. Further simulations to better quantify the degree of independence of the boundary resistances are presented in Appendix A.

Although our simulations provide strong evidence in favor of the assumption of splitting the total resistance as a sum of resistances [Eq. (9)], the fundamental process behind this behavior is still not well understood. In particular, the bulk mean free path of most of the phonons in each material composing the interface is larger than the length of the intermediate layer. This suggests that phonon-phonon interaction should play a negligible role defining the conductance of the system. Nevertheless, Figs. 2(a) and 2(b) show that the trend of G vs m_j in the anharmonic limit is different from that in the harmonic limit. Thus, it is clear that phonon-phonon interactions can be critical to phonon transport even across an intermediate layer thinner than the mean free path, but more research is necessary to understand the mechanism for this phenomenon.

V. CONCLUSION

We study the enhancement of thermal conductance when a thin film layer or junction is inserted at an abrupt interface. Our simulations show three times larger enhancement when

the harmonic approximation is relaxed, which highlights the important role of phonon-phonon interactions in this transport process. In fact, in the harmonic limit, adding a junction to the abrupt interface does not necessarily enhance the conductance. The result depends on the interplay between (1) increasing the transmission by improving the "matching" of the contacts and (2) decreasing the number of available transport channels that conserve energy and transverse momentum. When anharmonicity kicks in, the conservation constraints are relaxed and the resistance of the system can be split into the sum of boundary resistances. The resistance is minimized when the junction mass is the geometric mean of the contact masses, which follows from the increasing trend of the boundary resistance with mass ratio. The strategy to find the maximum conductance can be used beyond systems with perfect interfaces where only mass is changing. We hypothesize that for a graded junction the geometric mean result generalizes to an exponential progression of masses that can push the enhancement beyond that of a single layer. This paper exemplifies the powerful combination of Landauer and NEMD to study the harmonic vs the anharmonic contributions to thermal conductance.

ACKNOWLEDGMENTS

C.A.P., J.Z., and A.W.G. are grateful for the support from NSF-CAREER (QMHP 1028883) and from NSF-IDR (CBET 1134311). This work used the Extreme Science and Engineering Discovery Environment (XSEDE) [36] (DMR130123), which is supported by National Science Foundation Grant No. ACI-1053575. R.R and P.M.N. acknowledge the financial support of the Air Force Office of Scientific Research (Grant No. FA9550-14-1-0395).

C.A.P. and R.R. contributed equally to this work.

APPENDIX A: SIMULATION DETAILS

We calculate the thermal conductance between the left and right contacts of abrupt and bridged interfaces (Fig. 7). For each system, the crystal structure, lattice constant a, and interatomic force constants are invariant. The boundaries between adjacent materials are perfectly abrupt. The junction is six conventional unit cells long and the junction atomic mass m_j is varied between the contact atomic masses m_l and m_r. We simulate interfaces on FCC and DC crystal structures.

For the DC interfaces, the interatomic force constants are calculated from the Stillinger-Weber interatomic potential for Si [37]. This potential describes the energy in terms of two and three body potentials and includes interatomic force constants

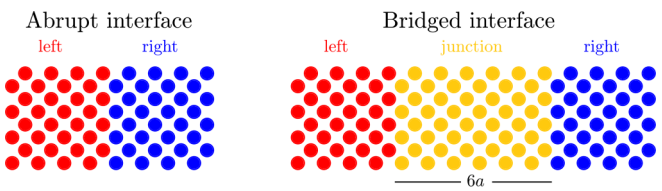

FIG. 7. Lateral view of the abrupt and bridged interfaces simulated in this work. Each ball represents a primitive unit cell.

up to the second-nearest neighbors. The equilibrium lattice constant for this structure is $a = 5.431$ Å at $\boldsymbol{T} = 0$ K. The mass for the left contact is chosen as the silicon mass $m_l = 28$ amu and the right contact mass is chosen as $m_r = 84$ amu, which is close to the mass of germanium. The conductance for the abrupt interface calculated from Landauer or harmonic NEGF in the classical limit is $G^A = 260.1$ MW m^{-2} K^{-1} [Fig. 2(c)]. This value is in good agreement with reported conductance values $G^A = 276.6$ MW m^{-2} K^{-1} at $\boldsymbol{T} = 300$ K [15] and $G^A = 280$ m^{-2} K^{-1} [13], which belong to abrupt interfaces with contact masses $m_l = 28$ amu and $m_r = 72$ amu. Our value is smaller because of the heavier mass on the right contact, which reduces the available phonon spectrum for conduction.

For the FCC interfaces, the interatomic force constants are calculated from the Lennard-Jones potential with parameters $\epsilon = 0.0503$ eV, $\sigma = 3.37$ Å, and a cutoff distance of 2.5σ. This potential includes interactions up to the fifth-nearest neighbors and is chosen to be identical to that used by English *et al.* [12] to have a point of reference for benchmarking. The equilibrium lattice constant for this structure is $a = 5.22$ Å at $\boldsymbol{T} = 0$ K. The mass of the left contact is fixed to $m_l = 40$ amu, while the mass of the right contact is varied from 40 amu to 240 amu. For Figs. 2(a) and 2(b), Fig. 3, Fig. 4(a), and Fig. 5(a), $m_r = 120$ amu. For Fig. 2(d), $m_r = 240$ amu. From harmonic NEGF in the classical limit, the conductance for the abrupt interface is $G^A = 59.3$ MW m^{-2} K^{-1}. This is in excellent agreement with the conductance from NEMD at $\boldsymbol{T} = 2$ K including the contact resistances $G^A = 61.0$ MW m^{-2} K^{-1}.

For the NEGF simulations, we take advantage of the transverse symmetry of the systems. We calculate MT in transverse wave-vector space ($k_\perp-$ space) to simplify the 3D problem into a sum of 1D independent problems. The transverse Brillouin zone was split into 50×50 grid points for both the FCC and DC crystals.

For the NEMD simulations we use the LAMMPS MD simulator on a system with $10 \times 10 \times 62$ conventional unit cells and a time-step of 2 fs. We impose periodic boundary conditions over x and y directions and set the atomic layers at the two ends of the system as walls. Heat is added to the system from the left edge and removed from the right edge using the Langevin thermostat. The baths temperatures are set to $\boldsymbol{T}_{\text{bath}} = (1 \pm 0.1)\boldsymbol{T}$ with a time constant of 1.07 ps over blocks of 10 unit cells length. This setup for the thermostat is done to ensure sufficient phonon-phonon scattering that prevents size effects. On the computations at very low temperatures ($\boldsymbol{T} = 2$ K), significant size effects can arise due to the lack of phonon thermalization. $\boldsymbol{T} = 2$ K corresponds to the nondimensional temperature $k_B\boldsymbol{T}/\epsilon = 0.003$, which is about 1% of the melting temperature. At such temperature, atomic displacements are small and atoms behave almost harmonically. Thus, phonon interactions due to anharmonicity are small and phonon thermalization is small. To obtain enough thermalization in our system, we increase the size of each thermal bath. We test for size effects by changing the cross section to 15×15 and 20×20, varying the length of the domain to 100 unit cells and decreasing the thermostat time constant to 0.54 ps. No significant change in the thermal boundary conductance is noticed. We also test for size effects on a bridged interface.

TABLE I. Size effects on the thermal conductance of a bridged interface obtained with NEMD. The junction mass is $m_j = 60$ amu, the contact masses are $m_l = 40$ amu and $m_r = 120$ amu, and the conductance is given in MW m^{-2} K^{-1}. Each column represents a different simulation domain with area and length given in unit cells squared (uc^2) and unit cells (uc), respectively. The standard deviation of five independent calculations is the value after ±.

Area (uc^2)	10 × 10	10 × 10	15 × 15	15 × 15
Length (uc)	60	120	60	120
$T = 2$ K	80.63±0.78	81.96	81.70	82.32
$T = 15$ K	105.38±1.17	106.91	105.80	107.51
$T = 60$ K	147.43±1.94	147.06	145.04	147.22

Table I shows that the relative change of conductance, when the cross-sectional area and length of the simulation domain increase from 10 × 10 to 15 × 15 unit cells squared and from 60 to 120 unit cells, respectively, is less than 2.1%. Considering that the standard deviation of the reported conductance values is about 1% (Table I), we can conclude that our results do not suffer from significant size effects.

To prevent changes of pressure as the temperature varies from affecting thermal transport at the interface, we account for the thermal expansion of the system. We perform equilibration runs under zero pressure at different temperatures using the isothermal-isobaric ensemble (NPT). The results are used to find the dependence of the lattice constant with temperature, which is fitted to a third order polynomial function:

$$a(T) = 5.2222 + 0.0004T + 10^{-6}T^2 - 4 \times 10^{-9}T^3 \text{Å}. \quad \text{(A1)}$$

Atoms are first equilibrated under the microcanonical ensemble (NVE) for 4 ns. Next, heat is added to the system for 10 ns to achieve steady state. Then, the temperature is recorded for 6 ns to ensure a proper statistical average. From the temperature profile, we estimate the thermal boundary conductance dividing the heat flux over the temperature drop, which arises from a linear fit of the temperature at each lead extrapolated to the interface.

Most of the conductance values from NEMD reported in this paper are averages over five independent calculations whose initial condition is generated randomly. The maximum conductances reported as asterisks on Fig. 6(b) are the maximum of fourth order polynomial functions used to fit the NEMD data.

The discrepancy in Fig. 6(b) between the maximum conductance of the bridged interface extracted from NEMD and the one predicted from Landauer can be attributed to the flattening of the G vs m_j curve around the maximum. Figure 8 shows the region (shaded area) where the enhancement of conductance is within 5% of the maximum enhancement. In that region, it is difficult to pinpoint the exact location of the maximum due to the uncertainty of the NEMD results. Nevertheless, the overall shapes of the Landauer and NEMD curves used to predict the maximum are in excellent agreement (Fig. 8). The different height between the curves is a consequence of the larger boundary conductances obtained with NEMD simulations [Fig. 2(b)]. The Landauer curve does not include the intrinsic resistance of the junction. Thus, its similarity with

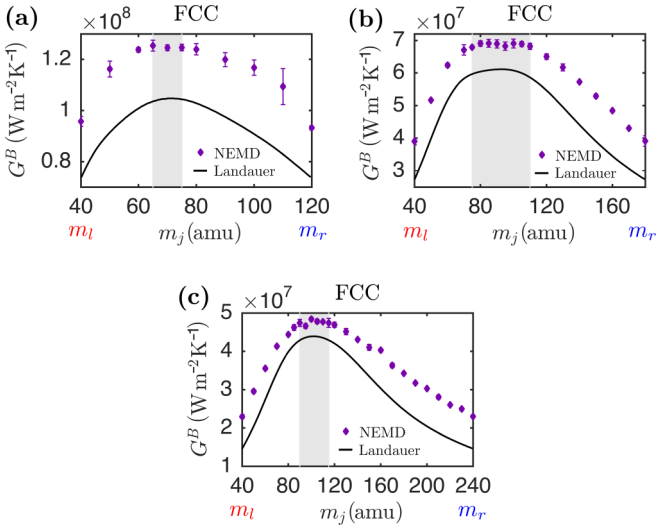

FIG. 8. Conductance vs junction mass for different right contact masses. (a) $m_r = 120$ amu, (b) $m_r = 180$ amu, (c) $m_r = 240$ amu. The shaded area shows the masses whose NEMD conductance enhancement is within 5% of the maximum enhancement. The Landauer curves come from Eq. (9) $-R_j$ using $\langle MT \rangle_\omega$ from Landauer [solid line Fig. 6(b)].

the shape of the NEMD curve in Fig. 8 suggests that individual boundaries play a dominant role in the maximization process. Thus, the quality of the conductance enhancement depends mostly on our ability to decrease the sum of the boundary resistances.

To further measure the degree of independence of the two layer-boundary conductances, we compare the conductance extracted from a simulation containing a single independent boundary with that extracted from a simulation containing two boundaries (Table II). Each NEMD simulation is labeled by the masses of the materials involved in the interface. For example, 40-60 refers to an abrupt interface with left contact mass $m_l = 40$ amu and right contact mass $m_r = 60$ amu, while 40-60-120 refers to an interface with $m_l = 40$ amu, intermediate layer mass $m_j = 60$ amu, and $m_r = 120$ amu.

TABLE II. Thermal conductance in MW m^{-2} K^{-1} from NEMD for a 40-60 and a 40-80 boundary at 30 K. The values in the left column are extracted from simulation containing a single boundary while the values in the other columns come from simulations containing two boundaries. The labels refer to the masses of the materials in the system, e.g., 40-60-120 have $m_l = 40$ amu, $m_j = 60$ amu, and $m_r = 120$ amu. Std. refers to the standard deviation of the mean conductance value over five independent calculations.

Conductance at the 40-60 boundary				
System	40-60	40-60-120	40-60-180	40-60-240
Mean	519.96	597.41	532.46	482.99
Std.	8.77	28.76	5.71	30.73
Conductance at the 40-80 boundary				
System	40-80	40-80-120	40-80-180	40-80-240
Mean	224.01	253.06	230.09	211.29
Std.	5.02	6.97	7.50	23.11

Table II indicates that the relative difference between the boundary conductances with and without the intermediate layer is less than 15%. Considering that the standard deviation of the calculations is about 5%, these values support the assumption that the resistances of each boundary are mostly independent of each other.

APPENDIX B: CONTACT RESISTANCE

According to Landauer theory, the conductance of a device in between two contacts at thermal equilibrium is defined by Eq. (1). When the device and the contacts are made of the same material, the transmission T equals one. In that case, we get the upper limit of conductance, which is proportional to the quantum of conductance times the number of propagating channels [30]. Since $T = 1$, there cannot be any resistance associated with the flow of phonons inside the device. Therefore, the maximum conductance measures the resistance at the contacts. This resistance arises from the implicit scattering processes that have to happen at the contacts, to bring the flowing phonons back to an equilibrium distribution [30]. The diffusive nature of those scattering processes allows us to split the resistance associated with the maximum conductance into the sum of the resistances at the contacts. Since for a homogeneous material those resistances should be equal, we can define the contact conductance in the classical limit as

$$G_c = \frac{2k_B}{2\pi A}\omega_c \langle M \rangle_\omega, \tag{B1}$$

with ω_c the cutoff frequency of the material and

$$\langle M \rangle_\omega = \frac{1}{\omega_c}\int_0^\infty d\omega M. \tag{B2}$$

The conductance from Landauer theory G_L is the parallel of the device conductance G_d with the contact conductances G_l and G_r, so the device conductance is given by

$$G_d = \frac{\left(\frac{G_l G_r}{G_l+G_r}\right)G_L}{\left(\frac{G_l G_r}{G_l+G_r}\right) - G_L}. \tag{B3}$$

Combining G_d with Eq. (10) we extract the $\langle MT \rangle_\omega$ referred as Landauer-R_{contacts} in Fig. 6(a). The method presented here is one way to approximate the contact resistances. Other approximations have been presented, which include an analogy to the four probe measurements [13,38].

From the temperature profile of the NEMD simulations when $\boldsymbol{T} \to 0$ [Fig. 3(b)], we can estimate the contact resistances, which are related to the temperature drops at the edges of the heat baths. At the contacts or heat baths, every time step the velocities of the atoms are rescaled to a thermalized distribution, which emulates phonon-phonon scattering processes bringing the region back to equilibrium. Everywhere else, phonons do not interact because the low temperature makes the system harmonic. Therefore, once a phonon leaves the contacts it cannot relax its energy creating a nonequilibrium distribution everywhere outside the bath regions. The temperature plotted in Fig. 3(b) is a representation of the total kinetic energy of the region with an equilibrium distribution.

The conductance measured from NEMD uses the temperature drop at the interface ($\Delta \boldsymbol{T}_{\text{i}}$), while the one measured from Landauer uses the temperature drop at the contacts ($\Delta \boldsymbol{T}_{\text{c}}$). Since the heat flux ($q = G\Delta \boldsymbol{T}$) crossing the system is the same, we can relate the conductances from the two methods with Eq. (2). Using this relation, we found excellent agreement between the results from Landauer and NEMD [Fig. 3(a)]. Another example supporting this relationship is shown in our recent work [34].

[1] D. G. Cahill, W. K. Ford, K. E. Goodson, G. D. Mahan, A. Majumdar, H. J. Maris, R. Merlin, and S. R. Phillpot, J. Appl. Phys. **93**, 793 (2003).
[2] W. Kim, R. Wang, and A. Majumdar, Nano Today **2**, 40 (2007).
[3] E. Pop, Nano Research **3**, 147 (2010).
[4] L. Shi, C. Dames, J. R. Lukes, P. Reddy, J. Duda, D. G. Cahill, J. Lee, A. Marconnet, K. E. Goodson, J.-H. Bahk, A. Shakouri, R. S. Prasher, J. Felts, W. P. King, B. Han, and J. C. Bischof, Nanoscale Microscale Thermophys. Eng. **19**, 127 (2015).
[5] P. E. Hopkins, ISRN Mech. Eng. **2013**, 19 (2013).
[6] D. G. Cahill, P. V. Braun, G. Chen, D. R. Clarke, S. Fan, K. E. Goodson, P. Keblinski, W. P. King, G. D. Mahan, A. Majumdar, H. J. Maris, S. R. Phillpot, E. Pop, and L. Shi, Appl. Phys. Rev. **1**, 011305 (2014).
[7] X. Li and R. Yang, J. Phys.: Condens. Matter **24**, 155302 (2012).
[8] X. Li and R. Yang, Phys. Rev. B **86**, 054305 (2012).
[9] R. J. Stevens, L. V. Zhigilei, and P. M. Norris, Int. J. Heat Mass Transf. **50**, 3977 (2007).
[10] Z. Liang and H.-L. Tsai, J. Phys.: Condens. Matter **23**, 495303 (2011).
[11] Z. Liang and H.-L. Tsai, Int. J. Heat Mass Transf. **55**, 2999 (2012).
[12] T. S. English, J. C. Duda, J. L. Smoyer, D. A. Jordan, P. M. Norris, and L. V. Zhigilei, Phys. Rev. B **85**, 035438 (2012).
[13] Z. Tian, K. Esfarjani, and G. Chen, Phys. Rev. B **86**, 235304 (2012).
[14] J. C. Duda, T. S. English, E. S. Piekos, T. E. Beechem, T. W. Kenny, and P. E. Hopkins, J. Appl. Phys. **112**, 073519 (2012).
[15] C. A. Polanco, R. Rastgarkafshgarkolaei, J. Zhang, N. Q. Le, P. M. Norris, P. E. Hopkins, and A. W. Ghosh, Phys. Rev. B **92**, 144302 (2015).
[16] C. S. Gorham, K. Hattar, R. Cheaito, J. C. Duda, J. T. Gaskins, T. E. Beechem, J. F. Ihlefeld, L. B. Biedermann, E. S. Piekos, D. L. Medlin, and P. E. Hopkins, Phys. Rev. B **90**, 024301 (2014).
[17] J. C. Duda, C. Y. P. Yang, B. M. Foley, R. Cheaito, D. L. Medlin, R. E. Jones, and P. E. Hopkins, Appl. Phys. Lett. **102**, 081902 (2013).
[18] P. J. O'Brien, S. Shenogin, J. Liu, P. K. Chow, D. Laurencin, P. H. Mutin, M. Yamaguchi, P. Keblinski, and G. Ramanath, Nat. Mater. **12**, 118 (2013).
[19] M. Jeong, J. P. Freedman, H. J. Liang, C.-M. Chow, V. M. Sokalski, J. A. Bain, and J. A. Malen, Phys. Rev. Applied **5**, 014009 (2016).

[20] J. P. Reifenberg, D. L. Kencke, and K. E. Goodson, IEEE Electron Device Lett. **29**, 1112 (2008).
[21] N. Faleev and I. Levin, J. Appl. Phys. **107**, 113529 (2010).
[22] C. A. Polanco and A. W. Ghosh, J. Appl. Phys. **116**, 083503 (2014).
[23] C. A. Polanco, C. B. Saltonstall, P. M. Norris, P. E. Hopkins, and A. W. Ghosh, Nanoscale Microscale Thermophys. Eng. **17**, 263 (2013).
[24] C. B. Saltonstall, C. A. Polanco, J. C. Duda, A. W. Ghosh, P. M. Norris, and P. E. Hopkins, J. Appl. Phys. **113**, 013516 (2013).
[25] E. S. Landry and A. J. H. McGaughey, J. Appl. Phys. **107**, 013521 (2010).
[26] C. Shao and H. Bao, Int. J. Heat Mass Transf. **85**, 33 (2015).
[27] M. Hu and D. Poulikakos, Int. J. Heat Mass Transf. **62**, 205 (2013).
[28] Y. Zhou, X. Zhang, and M. Hu, Nanoscale **8**, 1994 (2016).
[29] C. Jeong, S. Datta, and M. Lundstrom, J. Appl. Phys. **111**, 093708 (2012).
[30] S. Datta, *Quantum Transport: Atom to Transistor*, 2nd ed. (Cambridge University Press, New York, 2005).
[31] N. Mingo and L. Yang, Phys. Rev. B **68**, 245406 (2003).
[32] J.-S. Wang, J. Wang, and J. T. Lü, Eur. Phys. J. B **62**, 381 (2008).
[33] E. S. Landry and A. J. H. McGaughey, Phys. Rev. B **80**, 165304 (2009).
[34] N. Q. Le, C. A. Polanco, R. Rastgarkafshgarkolaei, J. Zhang, A. W. Ghosh, and P. M. Norris, arXiv:1610.01015.
[35] E. T. Swartz and R. O. Pohl, Rev. Mod. Phys. **61**, 605 (1989).
[36] J. Towns, T. Cockerill, M. Dahan, I. Foster, K. Gaither, A. Grimshaw, V. Hazlewood, S. Lathrop, D. Lifka, G. D. Peterson, R. Roskies, J. R. Scott, and N. Wilkens-Diehr, Comput. Sci. Eng. **16**, 62 (2014).
[37] F. H. Stillinger and T. A. Weber, Phys. Rev. B **31**, 5262 (1985).
[38] J. A. Katerberg, C. L. Reynolds, and A. C. Anderson, Phys. Rev. B **16**, 673 (1977).